Structure of tetracene films on hydrogen-passivated Si(001) studied via STM, AFM, and NEXAFS

A. Tersigni, J. Shi, D. T. Jiang, and X. R. Qin*
Department of Physics and Guelph-Waterloo Physics Institute, University of Guelph, Guelph, Ontario N1G 2W1, Canada
(Received 7 June 2006; revised manuscript received 7 September 2006; published 20 November 2006)

Scanning tunneling microscopy (STM), atomic force microscopy (AFM), and near-edge x-ray absorption fine structure (NEXAFS) have been used to study the structure of tetracene films on hydrogen-passivated Si(001). STM imaging of the films with nominal thickness of three monolayers (3 ML) exhibits the characteristic "herringbone" molecular packing known from the bulk crystalline tetracene, showing standing molecules on the *ab* plane. The dimensions and orientation of the herringbone lattice indicate a commensurate structural relationship between the lattice and the crystalline substrate. The corresponding AFM images illustrate that at and above the third layer of the films, the islands are anisotropic, in contrast with the submonolayer fractals, with two preferred growth directions appearing orthogonal to each other. The polarization dependent NEXAFS measurements indicate that the average molecular tilting angle with respect to the surface first increases with the film thickness up to 3 ML, then stabilizes at a value close to the bulk tetracene case afterwards. The combined results indicate a distinct growth morphological change that occurs around a few monolayers of thickness.

DOI: 10.1103/PhysRevB.74.205326 PACS number(s): 68.55.Jk, 68.37.−d, 81.15.Hi, 61.10.Ht

I. INTRODUCTION

Driven by their potential applications in future organic electronics, small aromatic molecules are attracting increasing attention.[1–3] They are of interest in fundamental studies of the organic electronics because many of these molecules could form high purity and well-ordered crystalline structures by sublimation techniques.[3] Tetracene is a planar aromatic molecule ($C_{18}H_{12}$) consisting of four fused-benzene rings [Fig. 1(a)]. The bulk crystalline structure of tetracene is layered herringbone molecular packing on the (001) plane [Fig. 1(b)].[4] Tetracene thin films prepared with vacuum sublimation have already been used to fabricate field-effect transistors (FETs),[5] and tetracene films have also displayed impressive properties in organic light-emitting FETs.[6] In order to achieve optimal material properties for these devices, the control of the film growth based on a good understanding is required. However, research on tetracene thin films is far from extensive. Theoretical studies on another polyacene, pentacene,[7] indicate that the bulk crystalline (001) facet has the lowest surface energy, and if the interaction between the molecules within a layer is much stronger than that between the molecule and substrate, as the typical case for the film growth on inert substrates, the film deposited is expected to exhibit the (001) orientation.[7,8] Given the similarities in pentacene and tetracene crystal structures, the above conclusions are likely applicable to tetracene. Studies aimed on increasing the mobility in tetracene thin films on silicon dioxide reported that the film growth is in favor of forming three-dimensional (3D) islands with a granular structure, and that the mobility limitation is primarily caused by the film growth properties.[9] Similar structural results were indicated by grazing incidence x-ray diffraction study that polycrystalline structures with polymorphs of different upright orientations of the molecules were found.[10] Until recently the layered morphology, similar to those in the pentacene film growth,[11–13] has been realized in tetracene film growth on a solid substrate.[14] A "layer-by-layer" growth was demonstrated for the tetracene films on hydrogen-passivated Si(001)-2×1 substrates within optimal range of deposition rates, and that good film connectivity and significantly improved grain size were obtained.[14] The Si(001)-2×1 surface used in this latter study provides a structurally well-defined [Fig. 2(a)] substrate template,[15] while the hydrogen passivation [Fig. 2(b)] removes surface dangling bonds[17] resulting in an inert substrate, leading to a well-suited surface for fundamental studies on the organic thin film growth.

Previous AFM results indicated that for a tetracene film deposited on H/Si(001) the molecules are in an upright standing configuration,[14] similar to that of pentacenes in weak molecule-substrate interaction cases.[7,8,18] However, more complete structural characterizations of the tetracene

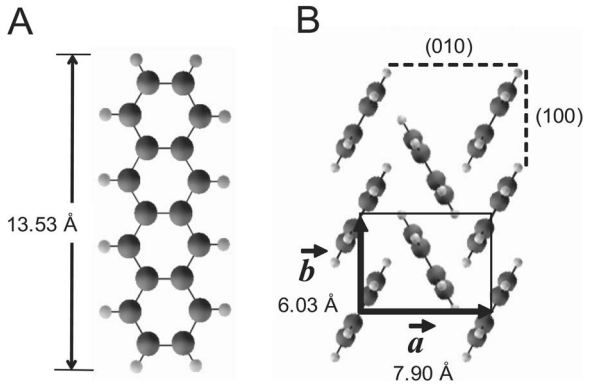

FIG. 1. (a) Schematic side view of a single tetracene molecule ($C_{18}H_{12}$) which consists of four fused benzene rings. C atom is shown in shaded black, and H atom in light gray. (b) Schematic top view (along the molecule long axis) of a single *ab* layer of tetracene in its bulk crystalline structure with two molecules in the unit cell.

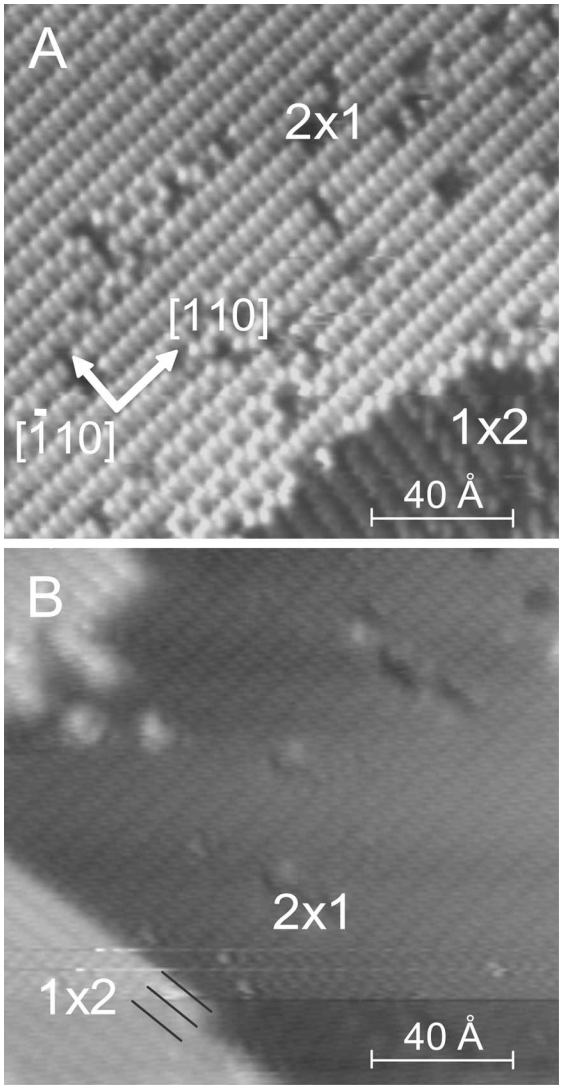

FIG. 2. Typical STM images (150 Å×150 Å) of (a) a clean Si(001) surface (filled state, at a bias of −2.0 V) and (b) monohydride-terminated Si(001) (empty state, +2.0 V), with a tunneling current of 0.2 nA. For both surfaces, the alternating 2×1 and 1×2 domains are energetically degenerate, with dimer rows running along the [110] and [−110] directions, respectively. The image of the monohydride Si(001) has the tunneling intensity minimums at the troughs between the dimer rows, as indicated by the dark lines in (b), clearly different from that for an empty-state image of a clean Si(001) under +2.0 V (see Ref. 16).

film are still not yet available. The structural properties of interest include the in-plane unit cell dimensions and possible registration with the substrate lattice and the molecule tilting angles, and in addition the evolution of these structural parameters with the film thickness. In this paper, we report a combined multitechnique investigation on these structural characterizations for the tetracene films. We show that the film of a few monolayers coverage possesses apparent epitaxial domains on the hydrogen-passivated Si(001) substrate with a bulk-kind herringbone lattice and a compressive in-plane lattice commensurate with the substrate. Also, the average molecular tilting angle with respect to the surface first increases with the coverage in forming the epitaxial domains and stabilizes around the bulk tetracene value in further growth. We associate the molecular-level structural information to a distinct growth morphological change that occurs around a few mononlayers of thickness.

II. EXPERIMENTAL DETAILS

A. Sample preparation and STM

The film growth and *in situ* scanning tunneling microscopy (STM) studies were conducted in a two-chamber ultrahigh vacuum (UHV) STM and growth system built in our laboratory.[19] The two chambers were isolated by a gate valve with base pressure $\sim1\times10^{-10}$ Torr for the STM chamber and $\sim3\times10^{-9}$ Torr for the growth chamber, respectively. Samples can be transferred between the two chambers in vacuum with a transfer arm.

In the STM chamber, Si(001) wafers were cleaned by thermal annealing. The Si substrate was resistively heated and the temperature was monitored by a *C*-type thermocouple in contact with the backside of the substrate. The *in situ* substrate cleaning procedure involves degassing the silicon wafer at 970 K and flashing at 1470 K for ~1 min, during which time the chamber pressure remained in the 10^{-10} Torr range.

Atomic hydrogen passivation was carried out with the silicon substrate at ~600 K. By dissociating molecular hydrogen (H_2) gas via a tungsten filament heated at ~1800 K, we generated atomic hydrogen inside the STM chamber by filling H_2 gas into the chamber at a pressure of $\sim1\times10^{-6}$ Torr for 30 min in order to form monohydride H/Si(001)-(2×1) surface.[20] The substrate was placed ~8 cm away from the tungsten filament. After the hydrogen passivation, the substrate was radiation cooled and transferred to the film growth chamber.

Tetracene (98%, Sigma-Aldrich) was evaporated in the growth chamber with the same setup and procedure described previously.[14] The deposition rate used was 1 nm/min, which was monitored by a quartz crystal microbalance. All the film growth was done with the substrate at room temperature. After film growth, the sample was then transferred back to the STM chamber for imaging.

The home-made STM (Ref. 19) uses a quadrant tube scanner and two inchworms for the *Z* and *X* coarse motion. Swartzentruber[21] type of control electronics and data acquisition software are adopted for the STM. All the STM images presented here were obtained in a constant-current mode. The sample bias used in imaging tetracene film was +2.4 V and tunneling current 20 pA.

B. AFM

After substrate preparation and film evaporation inside the UHV system as described above, the sample can be removed from the vacuum for other analysis via a load lock. Large scale topographic images were obtained by an *ex situ* atomic force microscopy (Digital Instruments Dimension™ 3100) in tapping mode with Si tips, and the images were analyzed using software WSxM.[22]

C. NEXAFS

Polarization dependent carbon 1s near edge x-ray absorption fine structure (NEXAFS) (Ref. 23) characterization was performed *ex situ* on the tetracene films with three different thicknesses (1.2 ML, 3 ML, and 15 ML) that were prepared using the growth system and procedure described above. Multiple samples for each tetracene film thickness were used and consistent results among the different batch of samples were obtained. The NEXAFS experiment was carried at the SGM beamline (11ID-2) at the Canadian Light Source (CLS) in Saskatoon, SK Canada. Total electron yield was used for the measurements under different beam incidence angles (θ) relative to sample surface. Sample fluorescence yield was monitored simultaneously using a multichannel plate detector and mainly used for signal diagnostic purpose in this experiment. The geometry for manipulating sample orientation with respect to the direction of the incoming synchrotron x-ray beam was the same as that in Ref. 23 and the NEXAFS measurements were conducted at room temperature. The SGM solid-state chamber vacuum was between low 10^{-8} to low 10^{-9} torr during the measurements. In order to avoid the effect of beam damage on the sample, each sampling area was used for one pair of the measurements at two incident angles (i.e., θ=90° and 10°) for about 10 min each. During the measurements, the CLS storage ring current was between 150 mA to 200 mA, and the monochromator entrance and exit slits were set to be 5 μm and 25 μm, respectively. The monochromator energy scale was calibrated by measuring CO gas phase C $1s \rightarrow \pi^*$ resonance energy at 287.40 eV (Ref. 24) during the same experimental run using a gas cell connected to the solid state chamber on the SGM beam line. The beam line optical transmission function was measured using a photodiode at normal incidence and the background data for the tetracene film samples were measured from a Si(001) wafer. The raw data background correction and normalization were carried out using the same multiple step procedure as that in Ref. 25.

III. RESULTS

A. Real-space imaging (STM and AFM)

Figure 3 displays the surface morphology of a tetracene submonolayer film on H-terminated Si(001) prepared as described in Sec. II A. As expected from our previous work,[14] the film islands appear as fractals under the growth conditions. The feature dimension is close to 100 microns [Fig. 3(a)], much larger than the value we obtained previously with a H-terminated substrate prepared using a wet chemistry method.[14] In Fig. 3(b) a close AFM examination reveals details of a fractal and also presents the morphology of the substrate with visible single atomic-layer steps that are oriented in random directions on the image scale. There is no clear indication of influence from these single-atomic-layer steps in the development of the fractal branches: branch splitting and extending occur on both local hills and valleys of the substrate. The heights of these submonolayer islands are measured using the AFM images, a value around ~1 nm is typically obtained [Fig. 3(c)], which is smaller than the length of the tetracene molecule (Fig. 1). This apparent layer thickness suggests that the molecules are essentially in an upright standing configuration in the submonolayer film but likely tilted away from surface normal direction.

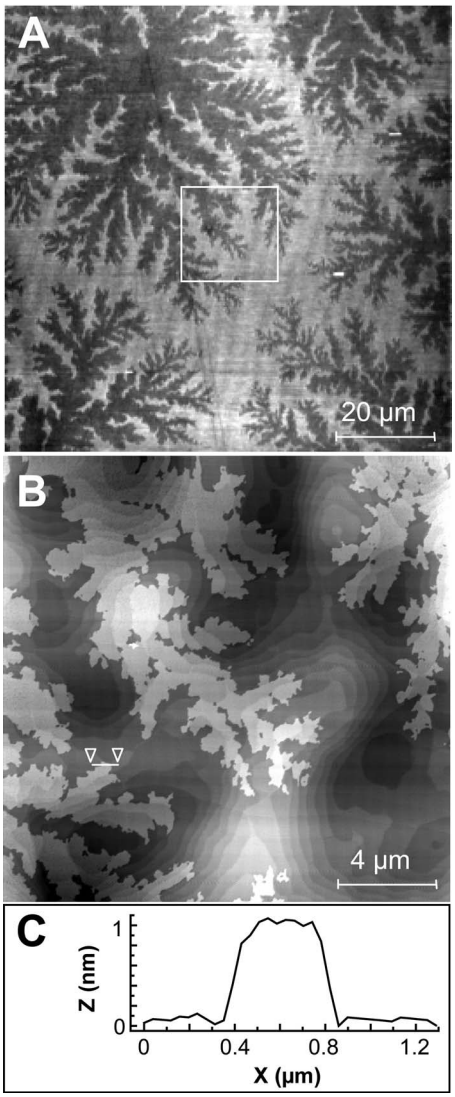

FIG. 3. (a) AFM phase image (100 μm × 100 μm) shows submonolayer tetracene fractals (dark feature). (b) A zoom-in topographic image (20 μm × 20 μm) of the area in the white frame of (a). (c) A line profile taken from the white bar marked by two triangles in (b) shows the height of ~1 nm for the layer.

To characterize the resulting structure of the fractal films at the molecular scale, efforts have been made to use our STM to image samples with either submonolayer coverage or with a coverage that has the top surface islands being the second molecular layer [i.e., the nominal thickness is ~1.2 ML (Ref. 14)]. So far no ordered structures have been imaged from the film surface at these coverages. We cannot exclude the possibility that the absence of molecular features in the STM image of the films is a result of the weak molecule-substrate interaction such that the soft film becomes susceptible to deformations induced by the STM scanning operations. On the other hand, the STM results could also indicate a possibility that there is a significant

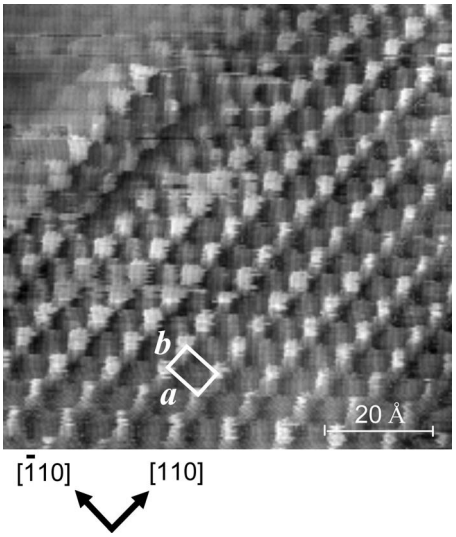

FIG. 4. STM image (85 Å×85 Å) of ~3 ML tetracene film on H/Si(001) surface. A rectangular lattice mimics the tetracene "herringbone" crystalline structure on the *ab* layer. The coordinates indicate that of the underlying substrate lattice orientations. The orientation of the herringbone lattice appears to follow the substrate lattice.

density of different molecular tilting domains that heavily disturbs the imaging of the domain structures. Because the fractal formation is largely based on diffusion-limited aggregation (DLA) (hit and stick) mechanism,[11,14] the as-grown first layer could be highly disordered.

Successful STM imaging of the molecular packing has been realized when we deposit three monolayer (ML) (nominal thickness) of tetracene onto the surface. Figure 4 shows a typical STM image of such films. The characteristic "herringbone" molecular packing known from the bulk crystalline tetracene is clearly visible, with the intensity protrusions indicating molecules in the image. The intensity protrusions form rows, with one row being brighter than its adjacent row in an alternating pattern, and the unit cell appears rectangular. Based on STM images of multiple independent samples, we calibrate the herringbone lattice (e.g., Fig. 4) as with $a=7.3\pm0.6$ Å and $b=5.5\pm0.6$ Å, closely resembling the *ab* unit cell dimensions of bulk crystalline tetracene (Fig. 1) within the uncertainty of the measurements. In other words, the STM image in Fig. 4 provides direct evidence that the film is crystallized with standing tetracene molecules on the *ab* plane on the inert substrate used.

Another striking feature of the STM image (Fig. 4) is that the bright rows (i.e., along the *b* axis) appear matching the substrate lattice orientation. With the same sample and imaging orientation settings as that used for the silicon substrate [Fig. 2(a)], the *b*-axis orientation imaged for the tetracene film in Fig. 4 appears precisely along the [110] direction as marked in Fig. 2(a) and Fig. 4. Among many STM images obtained, the orientations of the bright rows (along *b* axis in Fig. 4) are either as that shown in Fig. 4 or appearing orthogonal to it. Such film lattice orientation aligned to the crystalline substrate indicates that the molecules can recognize and lock into some specific structure sites on the substrate at this film coverage.

It is plausible that the herringbone lattice observed (Fig. 4) has a commensurate structural relationship to the substrate lattice. In addition to the orientation alignment between the molecular structure and the crystalline substrate as mentioned above, the calibrated spacing between the bright rows (i.e., the lattice constant measured along *a* axis) also matches well with the distance between the substrate monohydride dimer rows (7.68 Å) within the uncertainty of the measurements. Along the *b* axis (i.e., bright row) direction in Fig. 4, the lattice matching is not obvious, as neither substrate dimer spacing (3.84 Å) nor dimer row spacing (7.68 Å) match the *b* value. However, the multiple of *b* (e.g., 5 times as large) in principle could lead to a superlattice to match the substrate (as 5×6.03 Å$=8\times3.84$ Å$=4\times7.68$ Å). Though there is no visible superlattice modulation of image contrast indicated from our STM data, the existence of the superlattice cannot be excluded, as the modulation caused by the interface could be smeared out when imaged from a few molecular layers above.

Figure 5 shows an AFM image of a 3 ML tetracene film on a H-terminated Si(001) substrate. The image adds large-scale morphology information to what we learned from the STM data mentioned above. A line profile taken at the white bar (*AB*) is shown at the bottom of Fig. 5, indicating the height of ~1.4 nm for every layer including the buried first layer at the film-substrate interface. In contrast to the height measured on the fractal islands (Fig. 1), the first layer molecules in the multilayer regions must have had their orientations and packing rearranged to increase the tilt angle and hence the layer height in the growth. The line profile in Fig. 5 also allows a clear definition of the layers, we label them on the image with the second layer marked as "2," and the third layer as "3," etc. Since we never obtain any well-defined surface structure with STM when the films were prepared with only the first two monolayers presented, the molecularly resolved STM images (e.g., Fig. 4) most likely reflect the structure of the third or higher layer in the sampling surface area. Nevertheless, all the molecularly resolved STM images consistently show the surface symmetry as that in Fig. 4 and orientation registration to the substrate lattice discussed above.

The AFM image shown in Fig. 5 indicates that the film has a dramatic structure change and is highly crystallized on and after the third layer adsorption. First, the early third layer islands (Fig. 5) present two-dimensional (2D) dendrites with preferred branch orientations appearing perpendicular to each other, in clear contrast to the submonolayer fractal morphology (Fig. 2) that have randomly orientated branches. Second, there is a significant change on the nucleation density on top of the third layer: the density of the fourth layer islands is much higher than that of the previous layers (Fig. 6), exhibiting a lower surface diffusivity on the third layer. Third, the step-edge nucleation appears effective once the third layer is formed (e.g., as marked by an arrow in Fig. 5) that does not occur in the lower layers, indicating a structure change that causes Ehrlich-Schwoebel step barrier formed at the third layer edges. Finally, the formation of highly crystallized layers is consistent with our STM results that a well-ordered periodical lattice is presented on the surface. Compared to the film morphology in Fig. 6 with that in Fig. 3, it

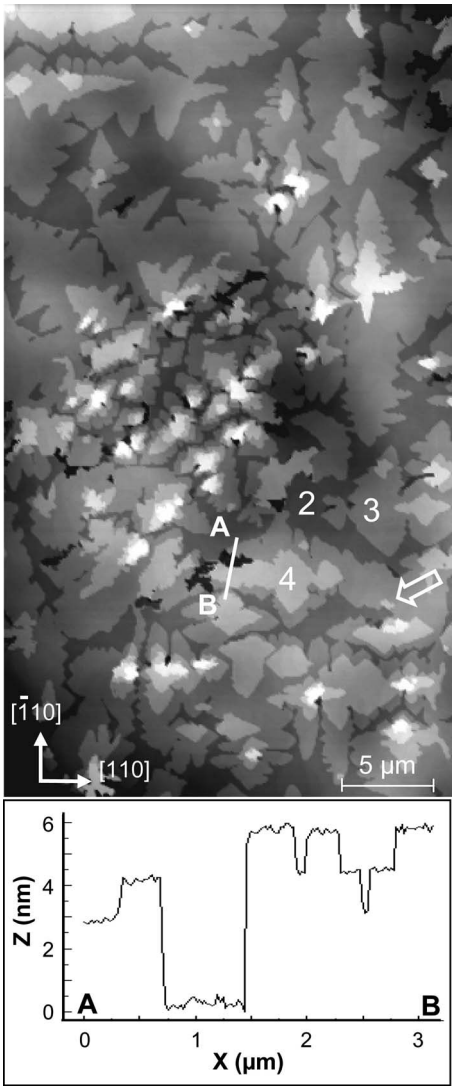

FIG. 5. AFM image (25 μm$\times$45 μm) of a 3 ML tetracene film on H/Si(001) with anisotropic tetracene islands on the third and higher layer. A line profile taken at the white bar (AB) is shown at the bottom, indicating the height of ~1.4 nm for each layer and suggesting the second, third, and fourth layers as marked by 2, 3, and 4 in the upper image, respectively. The coordinates indicate that of the underlying substrate lattice. An arrow marks a step-edge nucleation occurring on a third layer island.

is concluded that a growth mode change has occurred between these coverage stages.

In most cases, the orthogonal branched dendrites (i.e., the crosslike islands in Figs. 5 and 6) appear to have their two orthogonal branches oriented along the substrate domain directions (Fig. 6), i.e., along substrate [110] and [−110] directions, respectively. But, some dendritic islands rotated approximately 45° in azimuth angle away from the substrate lattice directions are also observed, as shown in the middle part of Fig. 5. Independent to which way the dendritic islands are oriented with respect to the substrate lattice, they always have their two main branch axes appearing mutually orthogonal. This structure character for the dendrites is not only consistent with what we have discussed that these third

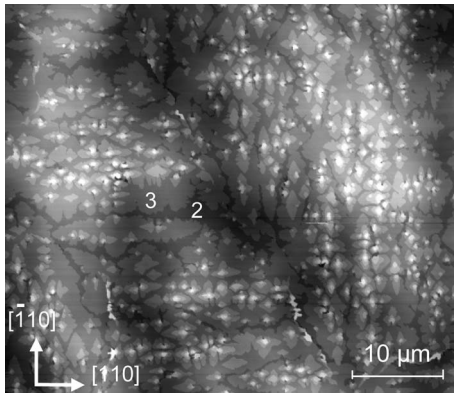

FIG. 6. Large scale AFM image (50 μm$\times$45 μm) of a 3 ML tetracene film on H/Si(001). Most of the anisotropic islands with their longer axes along substrate lattice orientations. The second and the third layers are marked by 2 and 3 in the image, respectively. The coordinates at the lower left corner indicate that of the substrate lattice.

layer islands are highly crystallized, but also indicating that their formation is mainly driven by molecular self-assembling. The fact that the majority of these surface islands follow the substrate lattice orientations (Fig. 6) suggests the existence of a non-negligible influence of the substrate lattice in the film nucleation and growth, presumably the commensurate registration is more energetically favorable.

The two apparently orthogonal orientations of the 2D dendrites shown on the third layer of the film are believed to be the herringbone lattice [010] and [100] directions (i.e., along the directions of b axis and a axis, respectively, in Fig. 1). Theoretical results on pentacene crystal show that the molecular binding energies (E_b) at the in-plane facets are in the following relation:[7] $E_b(010) > E_b(100) > E_b$ (other facets). The corresponding growth velocities of the (010) and (100) steps are thus relatively higher than the other facet steps,[7] i.e., the growth probability along the b axis is the highest and the a axis the second highest [see Fig. 1(b)]. If a similar binding energy relation is applicable to the case of tetracene due to the structural similarity between the two polyacenes, then the preferred island branch developments observed (Fig. 5) can be explained by the relatively higher growth probability along the b axis and a axis (which are close to orthogonal to each other), with the longer dimension being along the b axis.

B. X-ray absorption spectroscopy (NEXAFS)

To examine the interior structure of the film and how it evolves with the film morphology change discussed above, polarization dependent carbon 1s near edge x-ray absorption fine structure (NEXAFS) (Ref. 23) technique was applied. In this application the C $1s \rightarrow \pi^*$ photoionization resonance intensity (I_{π^*}) of the carbon atoms in the sample is measured, which varies with the relative orientation between the polarization of the incoming x-ray photon $\boldsymbol{\varepsilon}$ and the transition dipole moment ($\boldsymbol{P}$) of the molecules following the relationship $I_{\pi^*} \propto |\boldsymbol{\varepsilon} \cdot \boldsymbol{P}|^2$. The orientation of transition dipole moment

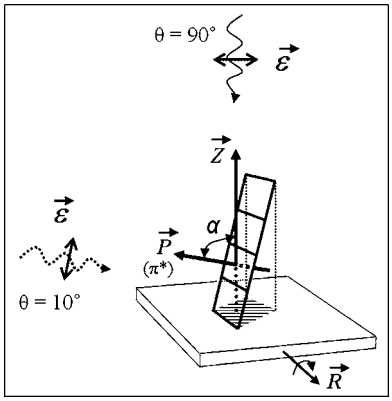

FIG. 7. Schematic view of the set-up geometry for the NEXAFS measurements. Tetracene molecule is represented by the rectangular grid sheet. The angle between the molecular transition dipole moment (***P***) (oriented normal to the plane of aromatic rings) and the substrate surface normal (***Z***) is the tilting angle α measured by NEXAFS. X-ray incidence angle (θ) with respect to the substrate surface is adjusted by rotating around ***R*** (x-ray direction is stationary in experiment). The linear polarization direction of the x ray is indicated by the vector $\boldsymbol{\varepsilon}$.

P for the π^* states of the aromatic rings is along the normal of the molecular plane. Therefore by measuring I_{π^*} at different x-ray polarizations (varying $\boldsymbol{\varepsilon}$) the orientation of ***P*** and hence that of the molecule with respect to the substrate can be deduced. In the current case the molecular orientation obtained represents an average over all the tetracene molecule layers.

The angular relationships among the various quantities involved in the NEXAFS experiment are illustrated in Fig. 7. For x-rays incident along the surface normal (θ=90°), an upright standing molecule such as the one schematically shown in Fig. 7 would yield strong π^* resonances, while for grazing-incidence x rays (θ=10°) the π^* resonance intensity would be minimized. Note that the angle α in Fig. 7 is the polar angle of ***P*** relative to the surface normal but there are two ways the molecular plane can be oriented to produce it: when the molecules are standing, e.g., as the case illustrated in Fig. 7; or when the molecule long axis lies in the plane and the molecule is rotated around its long axis. We exclude the latter case because the STM results shown in Fig. 4 and the AFM thickness estimates (Figs. 3 and 5) clearly indicate that through all the growth stages the molecules are in a standing orientation. Therefore, the bigger tilting angle α resulted from NEXAFS measurements indicates more upright standing orientation.

In general, the resonance intensity I_{π^*} may also depend on the azimuth orientation of the dipole transition moment relative to that of the x-ray polarization. However when the substrate lattice possesses a threefold or higher order of symmetry, the azimuth dependence of I_{π^*} vanishes.[23] Considering that the H/Si(100)-2×1 substrate possesses two degenerate reconstruction domains (2×1 and 1×2) orthogonal to each other, under the macroscopic sampling area covered by x-ray beam, the substrate surface would behave as if there is a 2×2 (fourfold) symmetry. Therefore in our case the NEXAFS of the tetracene films should be independent to the film azimuth orientation. This was confirmed by our NEXAFS measurements.[26] In this simplified high symmetry case, only two NEXAFS measurements at different x-ray incident angles (θ) are needed[22] for determining the average molecule tilting angle (α in Fig. 7). The resonance intensity can now be described by the following expression:

$$I_{\pi^*}(\theta,\alpha) \propto \frac{p}{3}\left[1+\frac{1}{2}(3\cos^2\theta-1)(3\cos^2\alpha-1)\right] + \frac{1-p}{2}\sin^2\alpha, \quad (1)$$

where $p=|E^{\parallel}|^2/(|E^{\parallel}|^2+|E^{\perp}|^2)$ is the degree of linear polarization in the plane of the synchrotron storage ring electron beam orbit and $E^{\parallel}$ and $E^{\perp}$ are the projections of the synchrotron x-ray in and out of electron orbit plane, respectively. For radiation from a planar undulator as the case in this study, the polarization is always linear if observed in the same horizontal plane of the insertion device center.[27] When considering various factors, the estimated uncertainty of θ using the current CLS SGM beam line setup is ±3°,[26] so the degree of linear polarization p is estimated to be in the range of 97% to 100%. The results on using either 100% or 97% for p differ less than 2° and this uncertainty will be included in the final α angle error bar to be reported below.

Figure 8 shows the typical NEXAFS data for the three tetracene film thicknesses, with beam at normal incidence and grazing incidence with respect to sample surface. The strong contrast in the π^* resonance intensity from the two beam polarizations indicates that all the films of different thicknesses possess a high degree of molecular orientation order. The overall spectral features in Fig. 8 are consistent with the results previously reported by Yokoyama *et al.*[28] for thick tetracene film measured at the magic angle, but with more detail resolved below the ionization potential (IP) around ~291 eV. The strongest resonance peak at 285.7 eV, which has been generally assigned as a C 1*s* to π^*-orbitals resonance in polyacenes,[29,30] has its energy location and intensity unchanged through the film thicknesses measured. This is actually the case for the other resolved features below IP as well.[31] Therefore chemically the molecules in all the films are similar to each other, which is consistent with the expected chemically weak influence of the film-substrate interface interaction.

Quantitative assessments on the molecular orientation require molecular orbital identifications of observed resonance features in Fig. 8. Theoretical study by Ågren *et al.*[29] has shown that the discrete resonance features in tetracene NEXAFS below the ionization potential consist predominantly in the split single π^* states of the excited carbon atoms. The spreading of the π^* resonance has been mainly attributed to energy and intensity variation of the resonance caused by the core-hole interaction effect (final state effect), and in addition to the site-dependent core ionization energy (initial state effect).[29,30] Similar conclusion as that of Ågren *et al.* was reached in a recent NEXAFS study of epitaxial growth pentacene films on Cu(110) surface by Söhnchen *et al.*,[32] where the discrete resonance features below the ionization potential were found to have an almost pure π^* charac-

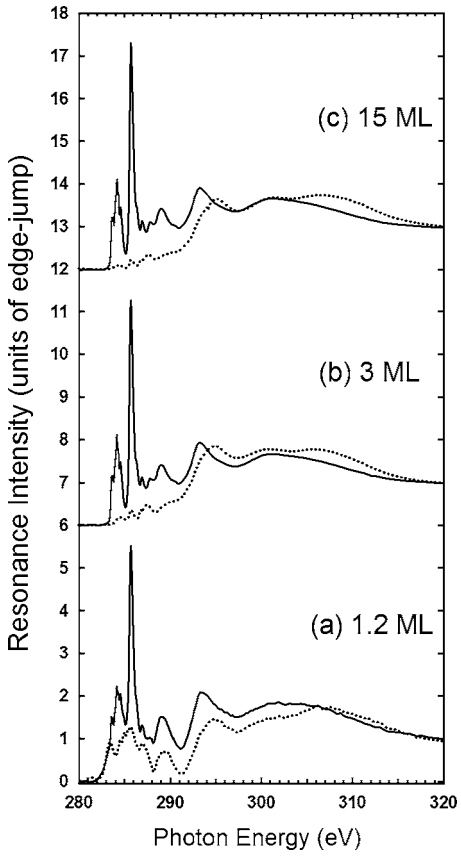

FIG. 8. Carbon *K*-edge NEXAFS data for tetracene films on H/Si(001). The film thicknesses are as marked in the figure. The data with x ray at normal incidence (θ=90°) and grazing-incidence (θ=10°) are shown by the solid lines and dotted lines, respectively. Data for 3 ML and 15 ML are shifted vertically for clarity.

ter. Based on these results, we treat all the resonance features below IP in Fig. 8 as due to π^* contributions (I_{π^*}), and the insignificant intensity with σ^* character from the tetracene end atoms[29] in this spectral region is neglected.[26] With these spectral assignments, the clear polarization dependence of the π^* states in Fig. 8 indicates that the molecules in these films are all in an upwards standing state. The area underneath the π^* resonances was integrated from 284.2 eV to 291.0 eV to obtain the measured resonance intensities at the two polarization angles and hence the experimental $I_{\pi^*}(\theta=10°)/I_{\pi^*}(\theta=90°)$ ratios (Table I). Using the expression (1), the theoretical $I_{\pi^*}(\theta=10°)/I_{\pi^*}(\theta=90°)$ ratio as a function of molecular orientation angle α is plotted, and

TABLE I. Determination of the average molecule tilting angle (α) between the molecular transition dipole moment and the substrate normal.

Thickness (ML)	Experimental $I(\theta=10°)/I(\theta=90°)$	α
15 ML	13.9%	78°±4°
3 ML	20.6%	74°±4°
1.2 ML	46.7%	65°±3°

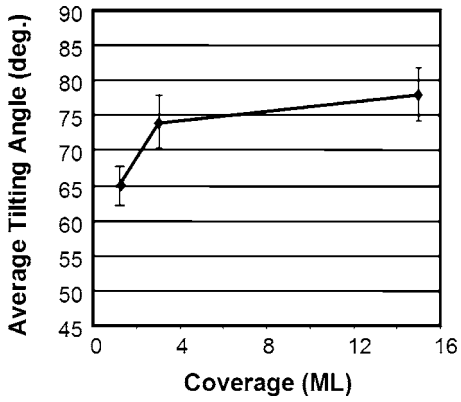

FIG. 9. The measured average molecule tilting angle (α) as a function of the film thickness. The line segments linking the points are only for visual aid purpose.

on this curve with an experimentally measured resonance intensity ratio the corresponding angle α is read out. Quantitative analysis of the data in Fig. 8 leads to the results of α varying as the film thickness, which is summarized in Table I and plotted in Fig. 9.

IV. DISCUSSIONS

Some insights about the structural evolution in the tetracene film growth on H/Si(100)-2×1 bore out by comparing the results from the three techniques applied, i.e., the lateral lattice orientation and dimensions given by STM, the interlayer separation or monolayer height and the morphology measured by AFM, and the molecular tilting angles as a function of the film thickness by NEXAFS.

For bulk tetracene crystal, the unit cell of the herringbone lattice on the *ab* plane consists of two molecules. With respect to the *ab* plane normal, these two molecules have their molecular plane normal oriented at angles of 81.9° and 70.1°, respectively.[4] Therefore, the average tilting angle of the two molecular-plane normals is 76° for the bulk tetracene crystal.[33] In other words, if measured by NEXAFS, the average tilting angle (α) for the bulk case would be 76°.

The NEXAFS data clearly indicate that the measured α of the tetracene film changes with increasing thickness (Table I and Fig. 9). For the 1.2 ML film, the average tilting angle is 65°±3°, well below the bulk case (76°). Considering the smaller height (~1 nm) obtained from AFM for the uncovered first monolayer and the corresponding result of nonordered structures imaged from STM, it is no surprise that the film exhibits a different molecular tilting angle from that of the bulk at this thickness. The obtained lower tilting angle in conjunction with the AFM and STM data suggests that the film is significantly disordered with an average molecular density lower than that in the bulk crystal.

At 3 ML nominal coverage, NEXAFS results indicate that the average tilting angle has increased significantly to 74°±4°, close to the bulk case value. STM and AFM also indicate significant structural changes at this film thickness: the molecularly resolved STM images exhibit ordered surface structures with commensurate relations to the substrate

lattice; and the AFM images illustrate drastic changes in the film morphology and a unified length for the monolayer height of each layer in the multilayer regions. We believe that these results from different techniques must be originated from a common structural evolution event. We attribute the significant increase of molecule tilting angle at 3 ML as due to the formation of the extended epitaxial domains (Fig. 4 and the anisotropic islands on and above the third layer in Fig. 5). Even though the STM imaging mostly shows the lattice symmetry of the top layer of the film, judging from the absence of any additional contrast modulation in the STM imaging, the difference in lattice symmetry between the top layer and the layer underneath is unlikely. In addition, the essentially same layer height for each layer in the multilayer islands shown by AFM (Fig. 5) indicates a vertical crystalline uniformity among the layers, including the first monolayer at the interface, which is consistent with our conjecture that the herringbonelike crystalline symmetry in Fig. 4 has been configured through all the layers forming the epitaxial domains. Comparing the lattice constants between a bulk tetracene crystal (a=7.90 Å) and the silicon substrate (dimer row spacing=7.68 Å), a laterally compressive film lattice is expected for the epitaxial domains. Apparently, in a laterally compressed epitaxial domain the molecules would stand more upright than in the bulk to accommodate the higher lateral packing density. The fact that the average titling angle for the whole film from NEXAFS is about the bulk value would require some molecules in the film having lower tilting angles. Two aspects may be accountable: (1) The areas where only two monolayers present in Fig. 5 are likely the modest tilting angle regions, as the ordered structures were not obtained from our STM measurements on top of a second layer; (2) from the film morphology shown in Figs. 5 and 6 there are terraced islands up to seven layers above the interface where the tilting angle for the upper layer molecules are expected, lower, as the film lattice is anticipated to be gradually relaxed along the distance away from the interface.

It appears that there is a structural phase transition associated with the film thickness. In addition to the presented data, we notice that the highly crystallized *islands* (i.e., the apparent epitaxial domains) emerge with the third layer formation on the surface from our AFM measurements.[34] The detail mechanism behind the phase transition is not clear. We speculate that with the increasing coverage more molecules may squeeze into the less densely packed first and second layers; the densification of the layers would enhance the intralayer molecular interaction and lead to a rearrangement on the packing and orientation towards the bulk configuration, and the influence of the substrate lattice remains somewhat effective, therefore resulting in the apparent epitaxial domains observed. Similar film coverage-dependent rearrangement of molecules was reported for physisorbed benzene on Ru(001) surface,[3,35] where the initially parallel oriented first physisorbed layer (above the parallel oriented first chemisorbed layer on the clean Ru surface) was found to rearrange into a more crowded layer with a high molecular tilt angle at higher coverages ($\geqslant$1 ML).[35] In the growth of tetracene on H/Si(001) in this work, the effect of the proposed molecule rearrangement and reorientation is significant at about 3 ML, and we believe that the apparent epitaxial domains (Fig. 4) are not formed initially at a lower coverage. The kinetics and the driving force of the structure transition require further investigations

After the drastic tilting angle change at 3 ML (Fig. 9), a new type of growth template appears on the film surface. Comparing to the fast increase of the molecule tilting angle from 1.2 ML to 3 ML, the further growth up to 15 ML introduces an insignificant increase in the molecule tilting angle (Fig. 9). The small average tilting angle increase, if meaningful, is likely related to the existence of nonepitaxial regions at 3 ML which are transformed to the epitaxial domains in the further growth. In fact at both 3 ML and 15 ML the average tilting angles (Table I) are basically in agreement with that of the average bulk value of 76°.

V. CONCLUSIONS

The structure of tetracene films on H-terminated Si(001), obtained under the optimized layer-by-layer growth process,[14] has been investigated by different structural probes (STM, AFM, NEXAFS). All the films investigated exhibit tetracene molecules in upright standing geometry on the *ab* plane. Under the film growth condition, the lateral packing for the molecules in the initial film is largely disordered. With increasing the film coverage to around 3 ML, a structural phase transition occurs which leads to the formation of apparent epitaxial domains with a commensurate structural relationship with the substrate lattice. From an abrupt increase in the molecular tilting angle in the film when approaching 3 ML coverage (NEXAFS) and from the compressive nature of the lateral film lattice (STM), it is suggested that the molecules in the epitaxial domains could be tilting more upright than in the corresponding bulk case. For the growth beyond 3 ML, the average molecule tilting angle levels around the bulk value.

ACKNOWLEDGMENTS

We gratefully acknowledge Brian S. Swartzentruber for valuable discussions and help in setting up our STM control system and John R. Dutcher for permitting our access to his AFM instrument for this study. D.T.J. would like to thank Tom Regier and Tom Koztzer for assistance in NEXAFS measurements at Canadian Light Source. This work was supported by the Natural Science and Engineering Research Council of Canada (NSERC), and by the Canada Foundation for Innovation (CFI) and the Ontario Innovation Trust (OIT). The operation of the CLS is supported by an NSERC MFA grant.

*Corresponding author. Email address: xqin@physics.uoguelph.ca

[1] S. R. Forrest, Chem. Rev. (Washington, D.C.) **97**, 1793 (1997).
[2] F. Schreiber, Phys. Status Solidi A **201**, 1037 (2004).
[3] G. Witte and Ch. Wöll, J. Mater. Res. **19**, 1889 (2004).
[4] R. B. Campbell and J. M. Robertson, Acta Crystallogr. **15**, 289 (1962); J. M. Robertson, V. C. Sinclair, and J. Trotter, *ibid.* **14**, 697 (1961).
[5] D. J. Gundlach, J. A. Nichols, L. Zhou, and T. N. Jackson, Appl. Phys. Lett. **80**, 2925 (2002).
[6] A. Hepp, H. Heil, W. Weise, M. Ahles, R. Schmechel, and H. vonSeggern, Phys. Rev. Lett. **91**, 157406 (2003).
[7] J. E. Northrup, M. L. Tiago, and S. G. Louie, Phys. Rev. B **66**, 121404(R) (2002).
[8] S. Verlaak, S. Steudel, P. Heremans, D. Janssen, and M. S. Deleuze, Phys. Rev. B **68**, 195409 (2003).
[9] F. Cicoira, C. Santato, F. Dinelli, M. Murgia, M. A. Loi, F. Biscarini, R. Zamboni, P. Heremans, and M. Muccini, Adv. Funct. Mater. **15**, 375 (2005).
[10] S. Milita, M. Servidori, F. Cicoira, C. Santato, and A. Pitteri, Nucl. Instrum. Methods Phys. Res. B **246**, 101 (2006).
[11] F.-J. Meyer zu Heringdorf, M. C. Reuter, and R. M. Tromp, Nature (London) **412**, 517 (2001).
[12] R. Ruiz, B. Nickel, N. Koch, L. C. Feldman, R. F. Haglund, A. Kahn, and G. Scoles, Phys. Rev. B **67**, 125406 (2003).
[13] G. Beernink, T. Strunskus, G. Witte, and Ch. Wöll, Appl. Phys. Lett. **85**, 398 (2004); S. Lukas, S. Söhnchen, G. Witte, and Ch. Wöll, ChemPhysChem **5**, 266 (2004).
[14] J. Shi and X. R. Qin, Phys. Rev. B **73**, 121303(R) (2006).
[15] M. P. Schwartz, M. D. Ellison, S. K. Coulter, J. S. Hovis, and R. J. Hamers, J. Am. Chem. Soc. **122**, 8529 (2000).
[16] X. R. Qin and M. G. Lagally, Phys. Rev. B **59**, 7293 (1999).
[17] J. J. Boland, Phys. Rev. Lett. **67**, 1539 (1991); J. Vac. Sci. Technol. A **10**, 2458 (1992).
[18] G. E. Thayer, J. T. Sadowski, F. Meyer zu Heringdorf, T. Sakurai, and R. M. Tromp, Phys. Rev. Lett. **95**, 256106-1 (2005).
[19] X. R. Qin (unpublished).
[20] Under the same atomic hydrogen dosing conditions but at lower substrate temperature, local 3×1 domains were observed on the surface, indicating that the dosing conditions are suitable to generate monohydride surface at the elevated temperature applied [see X. R. Qin and P. R. Norton, Phys. Rev. B **53**, 11100 (1996)].
[21] B. S. Swartzentruber, Phys. Rev. Lett. **76**, 459 (1996).
[22] WSxM©; http://www.nanotec.es
[23] J. Stöhr, *NEXAFS Spectroscopy*, Surface Science Series (Springer, 2003), Second Printing.
[24] R. N. S. Sodhi and C. E. Brion, J. Electron Spectrosc. Relat. Phenom. **34**, 363 (1984).
[25] S. Reiβ, H. Krumm, A. Nikiewski, V. Staemmler, and Ch. Wöll, J. Chem. Phys. **116**, 7704 (2002).
[26] D. T. Jiang *et al.* (unpublished).
[27] S. L. Hulbert and G. Williams, *Synchrotron Radiation Sources*, in Vacuum Ultraviolet Spectroscopy I, edited by J. A. Samson and D. L. Ederer (Academic Press, New York, 1998).
[28] T. Yokoyama, K. Seki, I. Morisada, K. Edamatru, and T. Ohta, Phys. Scr. **41**, 189 (1990).
[29] H. Ägren, O. Vahtras, and V. Carravetta, Chem. Phys. **196**, 47 (1995).
[30] H. Oji, R. Mitsumoto, E. Ito, H. Ishii, U. Ouchi, K. Seki, T. Yokoyama, T. Ohta, and N. Kosugi, J. Chem. Phys. **109**, 10409 (1998).
[31] Note: For the 1.2 ML grazing angle data in Fig. 8, the peak feature near the onset of the resonances ($\sim$283.5 eV) is likely due to the imperfection of the background correction scheme, not a real spectral feature.
[32] S. Söhnchen, S. Lukas, and G. Witte, J. Chem. Phys. **121**, 525 (2004).
[33] It should be noted that for tetracene the average tilting angle in NEXAFS is related to but different from the angle between the molecule long axis and the substrate surface plane, the latter for the bulk tetracene would be $\sim$68°.
[34] J. Shi, A. Tersigni, and X. R. Qin (unpublished).
[35] P. Jakob and D. Menzel, J. Chem. Phys. **105**, 3838 (1996).